Reda *et al. Bull Natl Res Cent (2021) 45:69*
https://doi.org/10.1186/s42269-021-00532-y

Bulletin of the National Research Centre

RESEARCH Open Access

Fortification performance of polyurethane coating in outdoor historical ironworks

Y. Reda[1], M. Abdelbar[2] and A. M. El-Shamy[3*]

Abstract

Background: Ironworks in the tomb of Suleiman Pasha Al-Faransawi (located in the old Cairo, Egypt) were exposed in the open-air are susceptible to various corrosion factors, which be contingent on the environmental conditions wherein the artifacts are displayed and the existence of a protective layer or not. Examinations and analysis were conducted to identify the structure and type of the alloys used in making the decorative ironworks, to identify the manufacturing technique and decoration, and to study the nature of rust compounds. This has been achieved by using metallographic microscopy, X-ray diffraction, and a carbon–sulfur analyzer. Many protection approaches have been worked such as varnishes, waxes, and oils, but they have had many disadvantages. The aim of this paper is to assess the competence of polyurethane coating by using electrochemical measurements (electrochemical impedance spectroscopy (EIS) and potentiodynamic polarization) in the fortification of ironworks exposed in the outdoor environment.

Results: The results confirmed that the decorative ironworks were manufactured from wrought and gray cast iron. The main corrosion products identified by XRD are goethite, akageneite, and maghemite. Lead oxide hydrate refers to old lead paints (red primer) which have been applied to protect the ironworks. Quartz and calcite are the products of heavy dust particles that covered the surface.

Conclusion: The data proved that the polyurethane is acting as a good protective coating for the decorative ironworks exposed in an uncontrolled environment. The 2% is considered as the recommended dose for this polymer for the minimum corrosion rate of the ironworks.

Keywords: Polyurethane coating, Ironworks, Surface characterization, Corrosion control, Conservation

Background

The main forms of iron alloys used historically are forged iron and cast iron (Taylor 2000). The wrought iron has a medium carbon content (not more than 0.35%); steel has a mild carbon content (between 0.6 and 2%), and cast iron has a high carbon content of more than 2% but usually less than 5% (Gayle et al. 1992; Scott 1991; Cronyn 1992). During the first half of the nineteenth century, cast iron was used as a structural and decorative building material, while after the eighteenth century, molded iron was used for small structural and even decorative elements. Steel introduced to the building industry in the late nineteenth century (Matero 1994; Bussell 2007; Mitchell 2009). Cast irons contain silicon, sulfur, phosphorus, manganese, nickel, and chromium, adding to carbon, and each of these fragments produces changes in the physical properties and the microstructure. In ancient history, the famous additives for the alloying process are Si, S, and P (Scott and Eggert 2009). Culturally, there have been two distinct cast irons: the gray cast iron with gray fracture entry, and the white cast iron with white fracture presence. Those irons with a mixed appearance of gray and white are called mottled iron (Bramfitt and Benscoter 2002). Due to its constituents and the techniques used in melting, casting, and heat

*Correspondence: elshamy10@yahoo.com
[3] Electrochemistry and Corrosion Lab., Physical Chemistry Department, National Research Centre, El-Bohouth St. 33, Dokki, P.O. 12622, Giza, Egypt
Full list of author information is available at the end of the article

treatment, the characteristics of several types of cast iron are categorized (US National Park Service 1991). Consequently, grey iron is the most common of all cast iron. Gray cast iron is the iron formula most frequently used in cast iron assemblies and architectural decorations of the eighteenth and nineteenth centuries (Donnelly 2009). Decorative architectural castings have historically been made using gray cast iron. The structure is crystalline and gives it excellent compressive energy, even if the tension is weaker (Davey 2013). For the reason that the carbon is occasionally decanted as thin fragments of graphite disseminated through the matrix, therefore, it is relatively brittle (Cardarelli 2008). The graphite is present as small nodules or flacks, which precipitate from random growth points in the cooling point. The manufacturing technique of ironwork elements was carried out by sand molding process which was essentially the same process that is used today, but with less automation (Howell 1987). In the case of wrought iron and steel, the cast iron is too hard, and brittle, and hammering, grinding, or pressing is unlikely to be suggested. Cast ironworks were often composed of several individual castings joined together. Cast iron was brought together without the applying of any welding at all, frequently by earnings of lugs, grooves, pins, and bolts. These joining performances are fragments of the character of cast ironwork. Riveting joints indicate either wrought iron or steel. Riveting was seldom used on cast ironwork as the driving and contraction of hot rivets risked fracturing the casting. Fire- or forge-welded joints that are heated white-hot and knocked together usually indicate wrought iron. Arc-welds indicate steel unless subsequently applied to earlier wrought iron, as the technique was not available when wrought iron was in widespread use (Campbell and Tutton 2013). Historic ironwork including wrought iron, cast iron, and steel has almost always been coated wherever it was used externally (Blackney 2002). Paint is commonly functional to ironwork items for two reasons; protective and decorative purposes. Paint is composed of powdered solid pigment providing color mixed into a fluid that cures or dries and bonds it to the surface. To regulate the viscosity and easiness of application, a solvent or 'thinner' is applied. A small group of pigments-red lead, iron oxide, tar, and graphite-continually reappear in discussions of metal primers in the nineteenth century (Hawkes 1979). Within the former, additional varnishes were also used for protecting iron, such as linseed oil (further shared use on sealed ironworks) and galvanizing (smearing a zinc layer). The tomb of Suleiman Pasha Al-Faransawi is in Cairo's old Cairo quarter, Mohammed Fouad Galal street, Egypt. It is a small cast-iron tomb in a residential square, it is lonely of Cairo's utmost unusual monuments, built in the nineteenth century (1860 AD) in honor of an extremely unusual man. Suleiman 'the Frenchman' was born in Lyon in 1788 (originally a soldier named Joseph Anthelme Séves). He was a veteran of campaigns by Napoleon who had come to Egypt to prepare viceroy Mohammed Ali's armies. The Frenchman, who died in Cairo in 1860, is said to have been so hated by his conscripts that they would kill him at target practice. Sèves later converted to Islam, taking the name Suleiman, and was rewarded with the honorary title "Pasha" following Egypt's successful campaigns against Greece and Syria. A statue of Suleiman mounted on his horse used to stand in Downtown Cairo on what was Suleiman Pasha street. During the 1952 revolution, the statue was transferred to the Salah Ed-Din Cairo citadel and the street renamed in honor of the Egyptian nationalist and banker, Talaat Harb (Thompson and Folkard 2001). The decorative ironwork was painted with red paints, the old paint underwent chemical alteration with air penetration as it was broken, flaked, and blistered, and thus required additional protective coats. So, the purpose of this inquiry is to appraise the efficacy of polyurethane coating to protect outdoor historic ironworks from corrosion by using electrochemical techniques polarization and impedance. Thermosetting polyurethane polymers are commonly employed as adhesives and sealants in a diversity of manufacturing requests outstanding to the wide range of physical and mechanical properties (Colson et al. 2015). Overall the years, ongoing work has been performed into appropriate materials for coating applications.

Materials and methods

Materials

Suleiman Pasha Al-Faransawi's Tomb was considered an architectural building and also a decorative medium. It has a column base, arches, windows, iron railings, and decorative ironwork. All the surfaces were coated with red primer except the lead which plated the dom, see Figs. 1, 2, 3, 4 and 5.

Methods

Metallographic examination

The metallographic examination was undertaken on a polished cross section through an OLYMPUS-PMT-VC2D03043JAPAN metallographic microscope. The small sample was reserved from the decorative units in the handrails. The cross section was prepared by embedding the sample in Bakelite and polished by using 600, 800, and 1200 grit emery papers, finally polished with diamond suspension (0.1 microns). The metallographic sample was etched using a 5% Nital etchant (5% HNO_3 and 95% ethanol) for 30 s.

Fig. 1 **a** Decorative ironworks exterior the Tomb of Suleiman Pasha al-Faransawi, and **b** decorative arches and columns

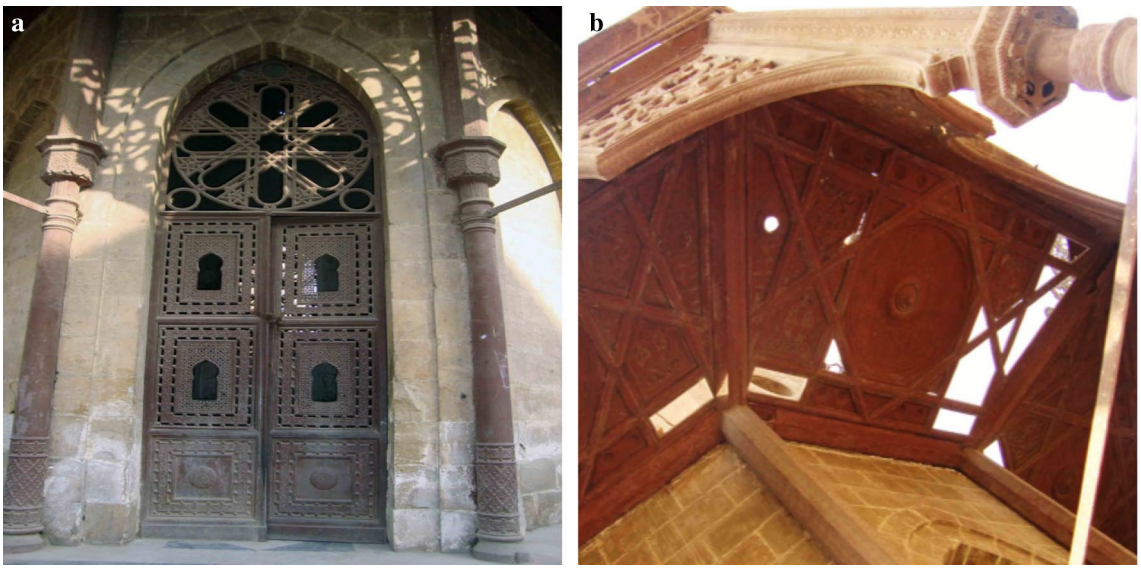

Fig. 2 **a** Main gate of the tomb and **b** missing parts in the roof

Carbon sulfur analyzer

The carbon and sulfur content of iron alloys used in the manufacture of decorative ironworks has been calculated using the ELTRA CS-2000 carbon sulfur analyzer. Two samples (0.5 g) were taken from the tomb's decorative units. The environmental conditions were: temperature: 21.5 °C, humidity: 33%.

X-ray diffraction

The weathering outcomes which fashioned on the superficial of the decorative ironwork units were identified using D8 advanced X-ray diffractometer (Bruker, Germany).

Fig. 3 Missing parts in the decorative column

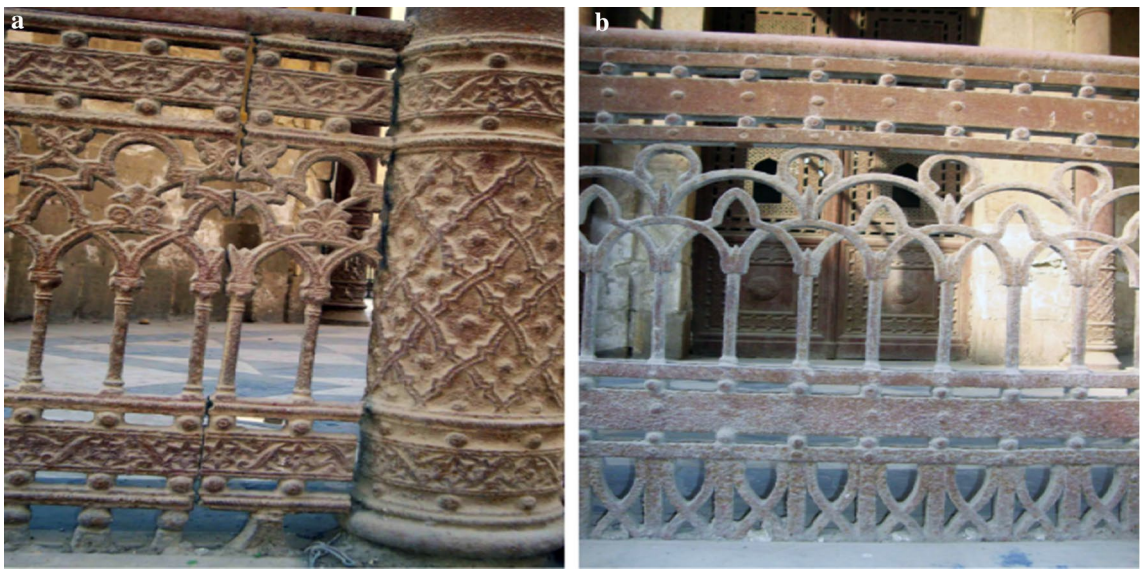

Fig. 4 Dust particles covered the fine details of the decorative iron railings

Coupons preparation

Preparation and processing of experimental iron coupons in the same manufacturing technique and the same natural structure of the decorative ironworks to evaluate the efficiency of polyurethane coating. The used material in this investigation is iron coupons of about 0.5 mm thickness with an immersed area of about 1 cm^2. The iron specimens were prepared by applying a methyl ethyl ketone as a degreaser for removing any oil or fingerprint on the specimens, in order to ensure the good adhesion of the followed applied coat. After ensuring the specimens are completely clean, the specimens were treated with alodine as a chemical conversion coating for the metal surface. After applying the alodine to the metal surface the metal color will change to yellowish-green, which ensures a good treatment of the surface. Within 72 h a polyamide epoxy primer was applied to the metal surface with an average coating thickness of 20 microns.

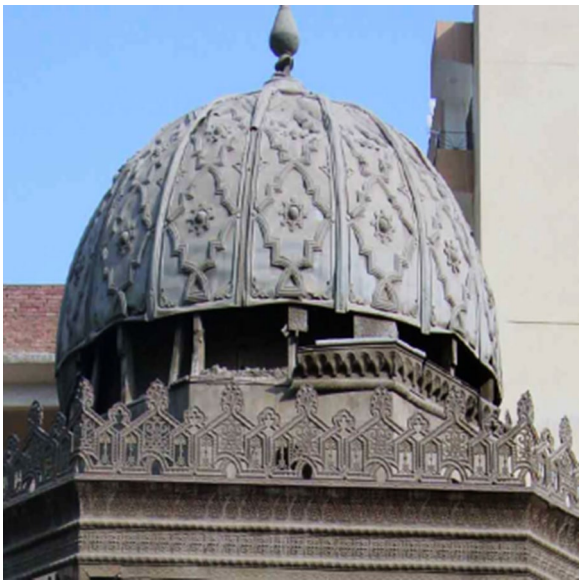

Fig. 5 Decorative lead Dom

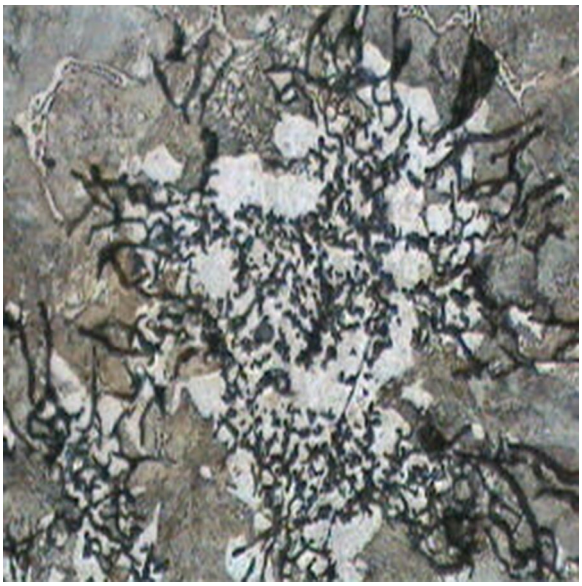

Fig. 6 Micrograph of a metallurgical structure consisting of ferrite (light constituent), pearlite (gray constituent), and graphite flakes (dark constituent). Etched in 5% Nital, × 200

Within 6 h—to avoid the complete sanding of the primer surface—a final coat of Nitro Cellulose Lacquer was applied on the epoxy polyamide primer with an average coating thickness of 40 microns or a final coat of polyurethane was applied on the epoxy polyamide primer with an average coating thickness of 60 microns.

Electrochemical studies

Electrochemical impedance spectroscopy (EIS) The electrochemical cell was a typical three-electrode Pyrex glass cell at room temperature using a computer-aided Autolabpotentiostat/galvanostat PGSTAT302N. A saturated calomel electrode as reference electrode a platinum foil was used as the counter electrode, aluminum alloy specimens coated and uncoated were used as electrodes. A total of 1.0 cm^2 area of the working operating electrode was uncovered to the 3.5% sodium chloride with and without stress. Before each experiment, the open circuit potential (OCP) was recorded for at least 30 min. The ac frequency range extended from 0.1 to 10^5 Hz. with a 10 mV peak-to-peak sine wave as the excitation signal. Electrochemical impedance spectra (EIS) were recorded at E_{corr} (i.e., at the stabilized OCP). All impedance data were fitted to an appropriate equivalent circuit.

The potentiodynamic polarization studies The potentiodynamic polarization studies were carried out in the same setup as that of electrochemical impedance studies. After electrochemical impedance measurements, polarization curves were recorded to study the effect of the coating films under stress and without stress on the efficiency of the alloy corrosion. All the polarization measurements were performed in the potential range from the cathodic to the anodic side (− 0.8 to 0.1 V) with scan rate 1.0 mV s^{-1} and at room temperature.

Results

Outcomes of the metallographic investigation of the manufacturing alloy of the decorative units of the first sample are given in Figs. 6 and 7. The results of carbon/sulfur analysis of the decorative ironworks are given in Table 1. The corrosion outcomes that formed on the decorative ironworks are categorized in Fig. 8 and Table 2. The OCP values were measured for 3000 s prior to the next electrochemical measurements as presented in Fig. 9. The polarization results for uncoated and coated iron electrodes with gradual concentrations of polyurethane in 3.5 wt% NaCl are accessible in Fig. 10. The collected parameters of potentiodynamic polarizations results, (OCP), (E_{corr}), Tafel slope (b_a and b_c), (I_{corr}), (CR), (IE%), and (R_p) are given away in Table 3. For more illustration, the *CR* and *IE %* are also calculated by using *EIS* and the obtained results are offered in Fig. 11 and the parameters between impedance and the amount of corrosion are mentioned in Table 4. Figure 12 represent the adsorption isotherms for polyurethane. Figure 13 shows more understanding about the adsorption of polymer on the iron surface, some kinetic models are considered for testing this behavior.

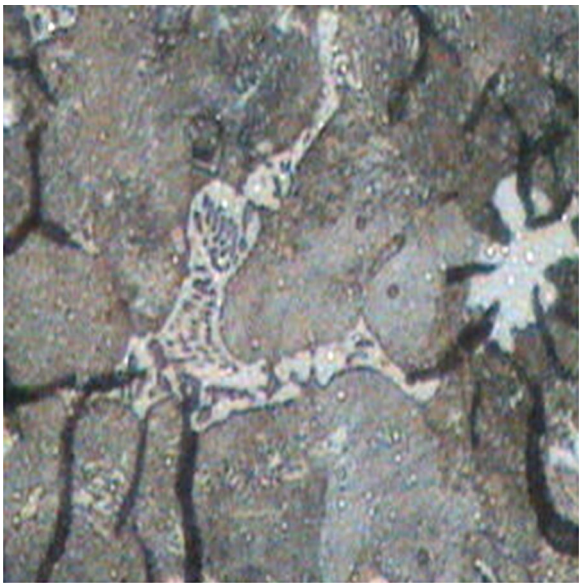

Fig. 7 Higher magnification represents graphite flakes, cementite, pearlite, and ledeburite. Etched in 5% Nital, × 500

Table 1 Results of carbon/sulfur analysis of the iron samples

Samples	Sulfur (wt%)	Carbon (wt%)
The first sample	0.08	3.53
The second sample	0.11	0.156

Discussion

Characterization of the decorative ironworks

An etched sample from the decorative ironwork units is shown in Figs. 6 and 7, represents the microstructure of the gray casted iron, consisting of a rosette grouping, the random orientation of ferrite (a light constituent), pearlite (a gray constituent), and graphite flakes (a dark constituent). This assembly is contingent on chemical configuration earlier the molding development, inoculants, and cooling circumstances (Behnam et al. 2010). Carbon is found in this alloy as graphite, which can take the form of flakes (gray cast iron) or spheres (spheroidal or spongy cast iron). In some instances, the carbon will be in the formula of iron carbide (cementite, Fe_3C) and the alloy was called white cast iron. Both forms of carbon make the casted iron a very brittle material, and thus, it was impossible to shape it by forging or hammering. Fortunately, outstanding to the lower melt points of cast iron, it was possible to melt the iron and cast it into the required shape (Barker 2006). In the gray casted irons, there is unrestricted carbon as graphite in the structure as some carbon content is rejected from solution and solidifying as flakes of graphite. Here are two important features manipulating the progress of graphite and cementite: solidification rate and composition. Since the iron–carbon phase diagram incorporating ferrite and graphite as stable products, it is the bordering to equipoise, sluggish conserving positive discrimination of graphite production, even though speedy cooling nepotisms the metastable ferrite and cementite system (Cronyn 1992). Therefore, this data confirms that the decorative ironwork units were manufactured from gray cast iron. The gained results of carbon/sulfur indicate that the decorative ironwork units were manufactured from cast iron alloy through carbon gratified of about (3.53 wt%) and sulfur (0.08 wt%). Gray cast iron comprises 1.7 to 4.5 wt% of carbon and other alloying elements such as Si, Mn, S, and P. Outstanding the deliberate chilling degree through casting, the carbon is occasioned as tinny fragments of graphite spread through the metallic lattice. Therefore, gray casted iron is relatively brittle (Cardarelli 2008). The second sample was wrought iron, through carbon gratified of about (0.156 wt%) and sulfur (0.11 wt%). Fashioned irons are practically unpolluted iron, with a smaller amount of about 1% (generally 0.02 to 0.03%) carbon. Slag diverges among 1% and 4% of their gratified and happens in a chastely physical suggestion, that is, it is not alloyed. This rigidity fashioned iron its distinctive bonded (covered) or tough assembly (US National Park Service 1991). Carbon steel is hard and straggly; it has the elastic properties and impacts resistance that bolts, beams, and girders need (Scott 1991). Wrought iron melts at 1535 °C (Barker 2006) and is remarkably malleable and generally ductile (unless it has been overworked and not annealed by re-heating), with similar strengths in tension and compression. The more wrought iron is worked the stronger it becomes; it is also easily welded. The final product can be a thing of beauty, as in the case of hand-wrought gates and grilles (Scott 1991). The microstructure of wrought iron is easily recognized, consisting primarily of ductile α–iron (ferrite) matrix with slag inclusion, mostly FeO and SiO_2. The slag is elongated during hot rolling, allowing the flow direction to be identified easily. Although the form of the severely deformed, the grains are not similarly elongated. Rather, they are roughly equiaxed, indicating that the ferrite recrystallized (Elban et al. 1998). The weathering crops determined by XRD analyses composed of goethite ($Fe_2O_3{\cdot}H_2O$), akaganeite ($Fe^{+3}O(OH)$), and maghemite (Fe_2O_3). Heavy dust particles can be recognized including quartz (SiO_2) and calcite ($CaCO_3$) forming thick crust layers. Lead oxide hydrate $PbO{\cdot}4H_2O$ was also identified. In the first limited hours of exposure onto the atmosphere, a moderately protective film of oxides and hydroxides forms

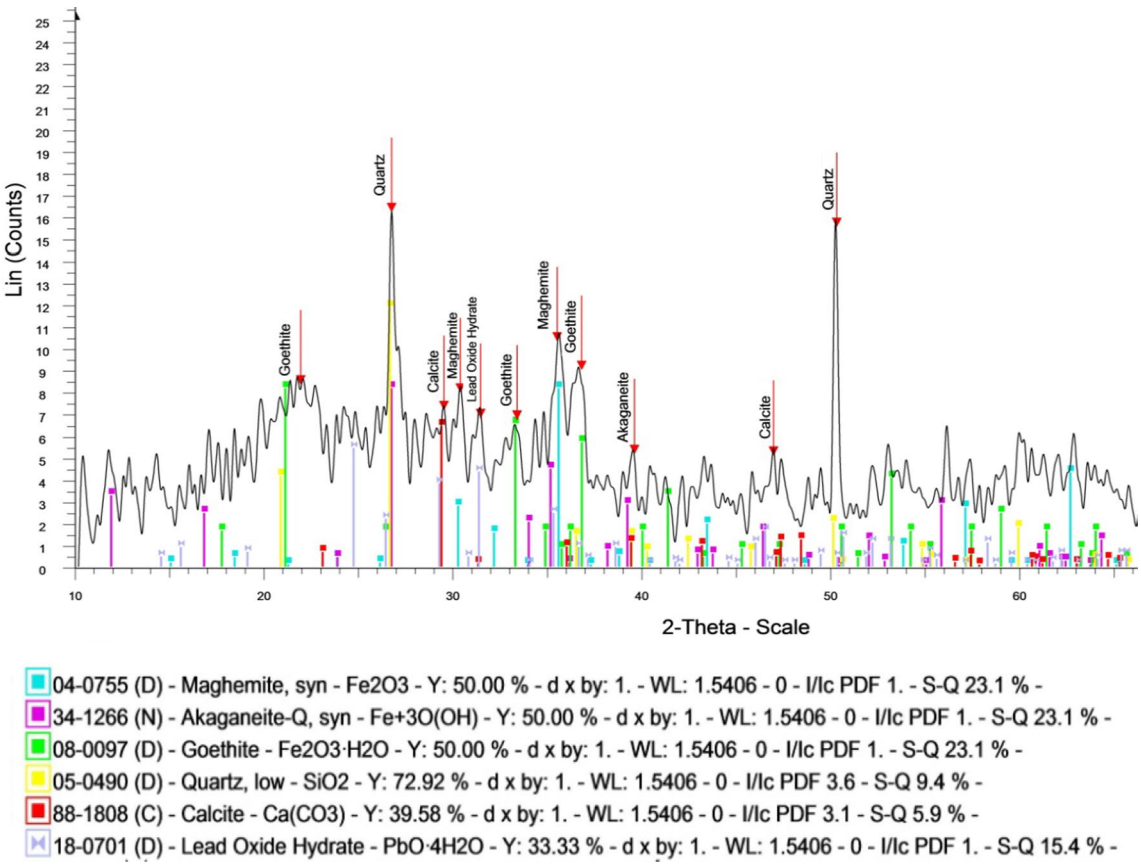

Fig. 8 XRD pattern of the corrosion products that formed on the ironwork units

Table 2 XRD results of the corrosion products that formed on the ironwork units

Card number	Compound	Chemical composition	Percentage	
34-1266	Akaganeite	$Fe^{+3}O(OH)$	23.1	Major
08-0097	Goethite	$Fe_2O_3{\cdot}H_2O$	23.1	
04-0755	Maghemite	Fe_2O_3	23.1	
18-0701	Lead oxide hydrate	$PbO{\cdot}4H_2O$	15.4	Minor
05-0490	Quartz	SiO_2	9.4	Traces
88-1808	Calcite	$CaCO_3$	5.9	

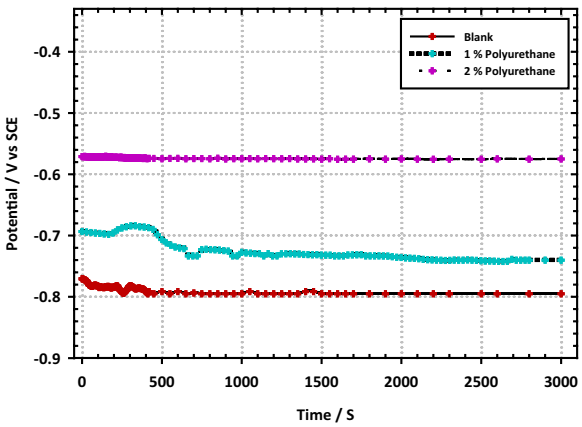

Fig. 9 Potential time variation of iron electrode in 3.5 wt% Na Cl and gradual concentration of polyurethane

(Scott and Eggert 2009). The rust layer that develops is porous, weakly adherent, and often cracked. Iron develops a layered structure of deterioration harvests over time. There is an innermost deposit of magnetite along with other amorphous iron corrosion products, and an external deposit of iron hydroxide oxides, typically goethite and lepidocrocite. The main reduction reaction supports the reduction of oxygen or iron decomposition. However, if the oxygen source to the metallic superficial is controlled by a build-up of iron hydroxide oxides, other reduction reactions become important. One possibility is the reduction process of

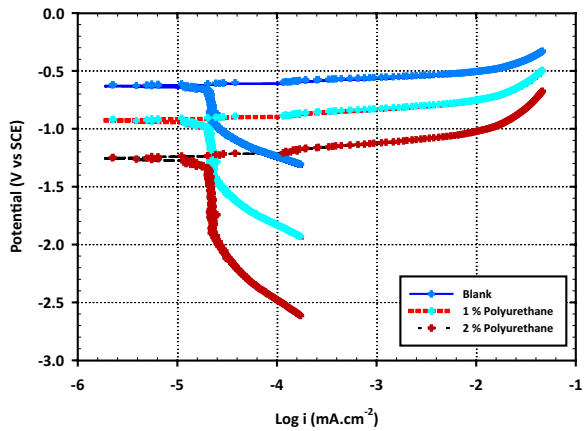

Fig. 10 Plots of potentiodynamic polarization of iron electrodes in 3.5 wt% of NaCl at gradual concentration of polyurethane

Table 3 Parameters of potentiodynamic polarization results cast iron in 3.5 wt% NaCl in the absence and presence of polyurethane at ambient temperature

Conc., (M)	β_a (V/decade)	β_c (V/decade)	i_{corr} (mA cm^{-2})	E_{corr} (mV)	I.E (%)
Blank	0.191	0.364	9.81	− 1.24 V	–
1%	0.161	0.252	1.72	− 946.2	83.7
2%	0.113	0.241	1.51	− 633.4	94.8

Fe^{3+} ions in existing iron hydroxide oxides to form an intermediate phase like iron (II) hydroxide (Selwyn 2004). Goethite (Fe_2O_3) is a significant primary corrosion product of iron objects and may form the principal corrosion product of freshly rusted surfaces or of iron artifacts that have been totally rehabilitated to weathering products. Akaganeite (ß-FeOOH) is an iron hydroxide oxide, which can be formed in chloride-rich environments, but as an iron corrosion product of a quite prevalent and usually implies active rusting of the iron artifacts (Logan 1995). The color varies from brown to bright yellow. Active corrosion generally can be identified by weeping, namely wet areas of acidic liquids, combined with the creation of brown corrosion products, known as akaganeite, which is characteristic of active corrosion. Maghemite (Fe_2O_3) has a red-brown color (Selwyn 2004). Cubic crystal is considered as one of the mutual products of rusting forms. It is widespread in nature and closely related to the changes that may occur to goethite and lepidocrocite during oxidation. It may form from the deliberate corrosion of magnetite or from lepidocrocite. The brown alteration product found on some magnetites near the surfaces has been acknowledged as maghemite. Maghemite can be made in one stage by thermal dryness of lepidocrocite. Goethite can be dehydrated to hematite and then reduced with hydrogen to form magnetite, which is oxidized to maghemite by the subsequent reaction:

$$2FeOOH \rightarrow Fe_2O_3 + H_2O \quad (1)$$

$$3Fe_2O_3 + 3H_2 \rightarrow 2Fe_2O_3 + 3H_2O \quad (2)$$

$$3Fe_2O_3 \rightarrow 2Fe_3O_4 + {}^1/_2O_2 \quad (3)$$

The presence of lead oxide hydrate ($PbO{\cdot}4H_2O$) could be ascribed to the occurrence of lead paints (red primer) which applied to guard the ironworks surface. Paint is normally used to ironwork for two explanations: the first is to shield the iron in contradiction of deterioration, and the second for attractive tenacities. In the nineteenth century, red lead was widely considered a priming pigment. A bright orange lead oxide guards against two types of corrosion. Second, since it is an alkali, it creates an appropriate basis along its surface of the metal and thus reduces the availability of hydrogen ions required for the corrosion-forming reaction. Its essential nature also allows the lead to bind to form the soap, lead linoleolate with the linseed oil, creating a film that is very durable, elastic and thus resistant to moisture. This reactivity produced several drawbacks. Some nineteenth-century painters felt that the chemical reaction between this oxide and the metal was truly galvanic and promoted rust. Though adding to its usefulness as a defender, the cementing reaction with oil has given it a limited shelf-life when sold as a pre-mixed coat. The pigment was expensive, making the paint both material-and labor-intensive because of its poor coverage. Finally, although initially solid, the paint was subject to chemical changes with atmospheric exposure, and hence, additional protective coats were required (Hawkes 1979).

Open circuit potential measurements

The OCP values were measured for 3000 s prior to the next electrochemical measurements, and Fig. 9 represents the gained results. Figure 9 shows the potential values for uncoated and coated cast iron coupons engrossed in 3.5 wt% NaCl with a gradual concentration of polyurethane. It clearly noticed that the potential shifted to more positive values with the rising of polymer concentration. The *OCP* values ranged from − 738 and − 575 mV at 1% and 2%, respectively, which indicates that the polymer is successful in mitigation of the weathering of the iron surface. It is found that the 2% of polymer shows great inhibition efficiency against chloride attack on iron superficial. So, the 2% is considered as the recommended dose for this polymer in this electrolyte for this iron alloy.

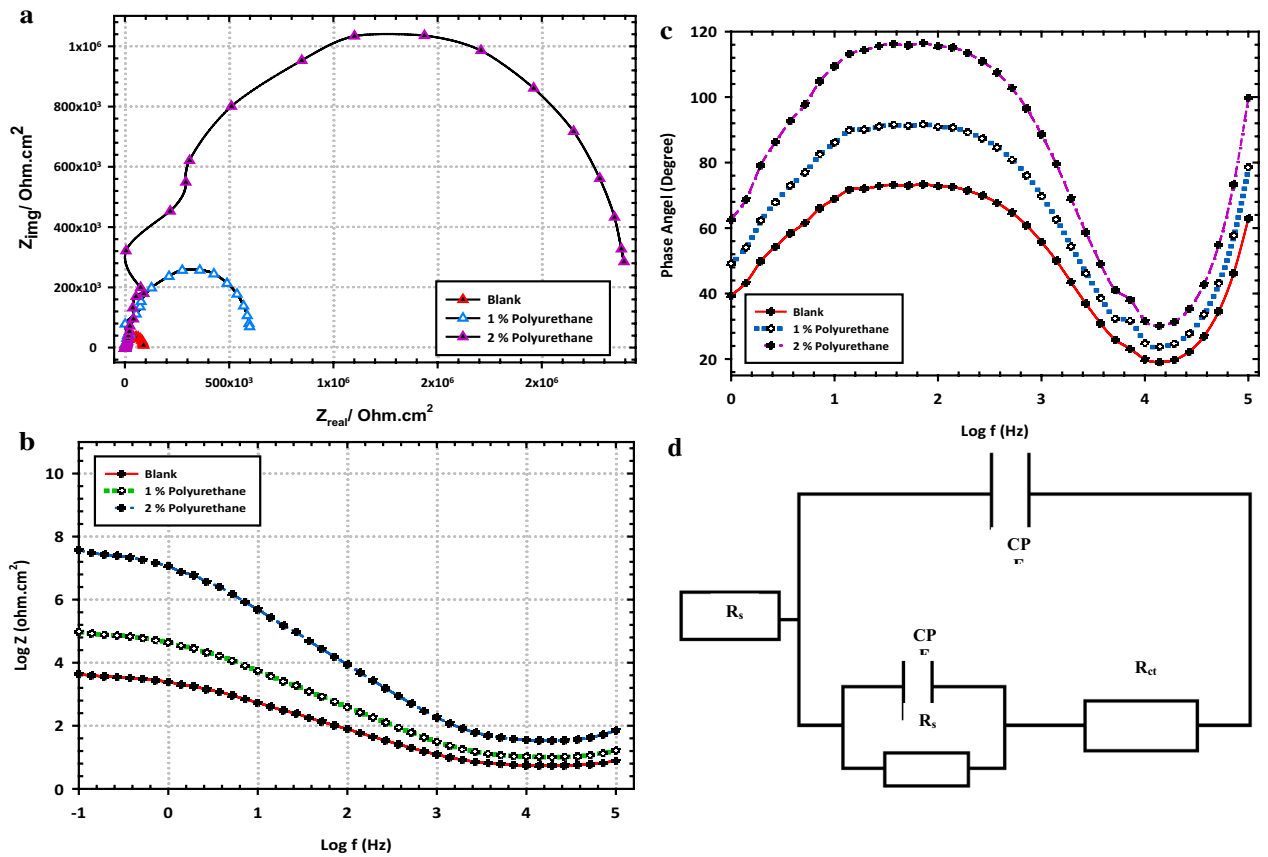

Fig. 11 EIS plots for cast iron in 3.5 wt% NaCl in the absence and presence of different concentrations of polyurethane at ambient temperature **a** Nyquist plots, **b** Bode plots, **c** phase angel, and **d** equivalent circuit

Table 4 Parameters of electrochemical impedance results for cast iron in 3.5 wt% NaCl in the absence and presence of different concentrations of polyurethane at ambient temperature

Conc. (M)	R_s (Ω)	CPE (μF cm^{-2})	α_1	R_{ct} (KΩ cm^2)	CPE_{ad} (μF cm^{-2})	α_2	R_{ads} (Ω cm^2)	R_T (Ω cm^2)	CPE_T (μF cm^{-2})	I.E. (%)
Blank	2.87	360.0	0.92	0.21	219.2	0.92	0.35	0.71	590.9	–
1%	3.24	280.0	0.88	2.3	154.1	0.89	2.89	4.95	420.0	87.9
2%	4.28	260.0	0.84	2.9	110.7	0.82	4.56	7.86	380.0	93.8

The agglomeration phenomenon is not noticed in this case so the polymer could be employed in a successful way of spreading on the metal superficial without any defect in the polymer layers.

Potentiodynamic polarization measurements

The polarization results for uncoated and coated iron electrodes with gradual concentrations of polyurethane in 3.5 wt% NaCl are accessible in Fig. 10. The results show that the current density values are decreased with growing the polymer concentration, which proves that the polyurethane is acting as a good coating for iron artifacts in saline media. This behavior is convenient and clears about 2% of polyurethane as publicized in Fig. 10. In addition, by snowballing the polymer concentration to 2%, the potential is shifted to the positive direction in addition to the current density is decreased which means that the coating has succeeded to make protection as elucidated by the creation of the adsorbed inhibitor molecules on the electrode surface. These results agreed with the OCP measurements. The collected parameters of the potentiodynamic polarizations results, (OCP), (E_{corr}), Tafel slope (b_a and b_c), (I_{corr}), (CR), (IE%) and (R_p) are given away in Table 3. These parameters proved

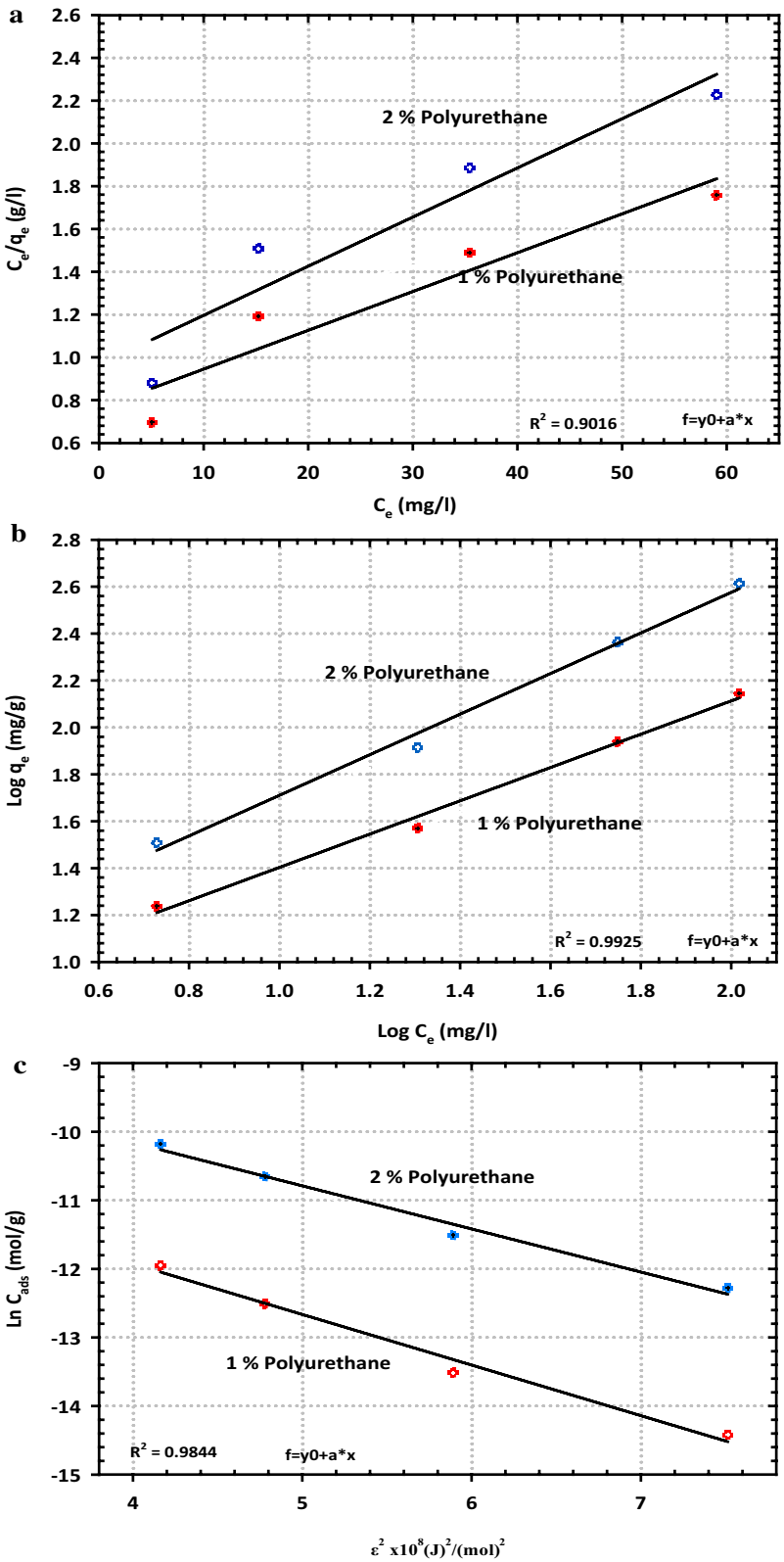

Fig. 12 Adsorption isotherms for polyurethane **a** Langmuir, **b** Freundlich and **c** Dubinin–Kaganer–Radushkevich

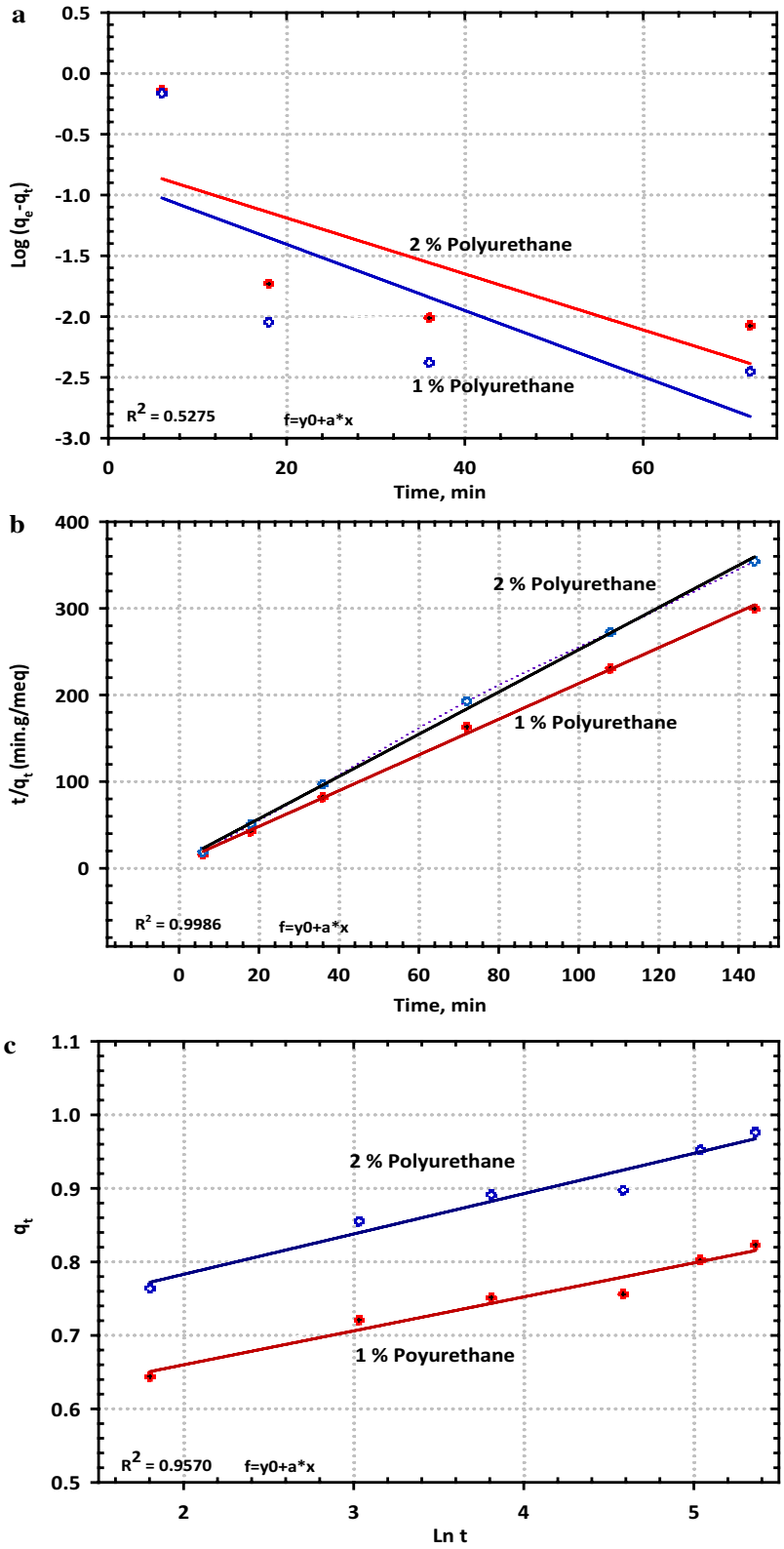

Fig. 13 Kinetic models of polyurethane **a** pseudo-first-order, **b** pseudo-second-order and **c** Elovich kinetic model

that the minimum corrosion rate with higher efficiency is obtained at 2% of inhibitor concentration. The IE% of higher 90% is considered highly promising results for field application. This high efficiency may be outstanding to the attraction between the polymer and the electrode surface by electron density of the N and O atoms.

Electrochemical impedance measurements

For more illustration, the CR and IE % are also calculated by using EIS and the obtained results are offered in Fig. 11 and the parameters between impedance and the amount of corrosion are mentioned in Table 4. All these tools proved that the best dose with higher inhibition efficiency and higher impedance is 2% polymer concentration. Figure 11a shows the Nyquist plot for a gradual concentration of polyurethane in 3.5 wt% NaCl solution, at high to intermediate frequencies, exhibits a characteristic semicircle that represents a transference of charge and capacitance double layer (C_{dl}) that occurred during initial film formation. The impedance increased with increasing polymer concentration until 2%, indicating that the inert coat created on the metallic superficial is more protective (Abdel-Karim et al. 2018). Figure 11b displays the Bode plot and it is a great fit and identified that the obtained variation proved that a defensive coat created on the electrode surface and approximately full protection against chloride attack is formed and the short spike that appeared at the lower frequency, suggests that the diffusion-limited process started at the metal–solution interface (El-Shamy et al. 2016). It is clearly noticed that as the rust layer increases in thickness less adherence and diffusion occurred (Reda et al. 2018, 2020). Figure 11c shows the Bode phase for different concentrations of polyurethane in 3.5 wt% NaCl. The Bode map (log *f* vs. log lZl) indicates an intermediate frequency capacitive region and a high- and low-frequency resistor zone. We noticed the impedance increasing as the concentration increased. The maximum phase at the intermediate frequencies increases with the upsurge of the polyurethane concentration, which indicates that the development of a protective layer and decreases at 2% polymer concentration. These results proved that the optimum concentration of about 2% from the polyurethane (El-Shamy et al. 2020). From the Bode-phase plot (log *f* vs. phase) it is observed that the rise in polymer concentration results in a rise in phase angle with a change to a low frequency which reached a maximum of 2%, suggesting corrosion inhibition. Figure 11d represents Randle's equivalent circuit model. The impedance circuit showed the (R_s) solution resistance in sequences through the corresponding amalgamation of (C_{dl}) double-layer capacitance and the (R_{ct}) charge transference resistance with (Z_w) Warburg impedance in series. The corresponding circuits were performed by appropriating the data with Nova software. Table 4 illustrates that the obtained fits with the improved Randle's circuit with impedance records for iron artifacts in the absence and the presence of polyurethane. R_{ct} grows with snowballing the polymer concentration up to the best concentration indicating the increased corrosion inhibition (Zohdy et al. 2019). The drop in the double-layer capacitances C_{dl} with the rise in polymer concentration can be attributed to the increase in the adsorption of inhibitor molecules on the oxidizing surface, which decreased the cumulative loads in the double layer and improved layer width and inhibition performance (Akindoyo et al. 2016). The findings obtained from the potentiodynamic polarization distributions were accepted with the impedance measurements as the (EIS) is an important tool for confirming the pathways of degradation and the adsorption hypotheses (Makar et al. 2001).

Adsorption isotherm and kinetics

The obtained results of polarization and impedance data show that polyurethane inhibits the weathering of the iron artifact through the adsorbed film at the surface. Adsorption of polymer involves physical adsorption by, electrostatic interaction with the metal surface and chemisorption involving the charge sharing between polymer molecule and metallic superficial through N and O atoms, and π electron of the aromatic ring as a donor and vacant *d*-orbital of iron as acceptor. Different adsorption isotherms can be investigated for metal interaction with inhibitor, and the experimental facts tailored the Langmuir Freundlich, and Dubinin–Kaganer–Radushkevich (DKR). Figure 12a represents the Langmuir isotherm the C/q_e versus C_e, and the gained results are fitted this isotherm with a moderate degree since the $R^2 = 0.9016$. The Freundlich isotherm represents the relation between log C_e and log qe and the obtained data were agreed carefully with this model as $R^2 = 0.9925$ as cited in Fig. 12b. The third isotherm Timken isotherm describes the relations between ln C versus $\mathcal{E}^2$ as mentioned in Fig. 12c. The straight line and the strong correlation value of $R^2 = 0.9844$ are obtained. The isotherms indicate that polyurethane obeyed Freundlich, Timken isotherm, and Langmuir as the correlation coefficients are $R^2 = 0.9925$, $R^2 = 0.9844$, and $R^2 = 0.9016$, respectively. In addition, the K values were mathematically calculated from the gained straight lines and proved that the rate of adsorption isotherm equilibrium constant is higher than 1 indicating the strong adsorption of polymer on the iron surface. The adsorption free energy ΔG can be calculated from the succeeding formula (Shehata et al. 2020).

$$\Delta G^{o}_{ads} = -RT \ln (1000 K_{ads}) \quad (4)$$

where 1000 is the concentration of water in solution gl^{-1}, R is the general gas constant 8.314 (J mol^{-1} K^{-1}), and T is the absolute temperature (K). It is well established that the values of ΔG^{o}_{ads} determine the adsorption category. The larger values of ΔG^{o}_{ads} in negative value and the higher stability of adsorbed layer of the polyurethane on the iron artifact surface with the formation of a coordinate-type bond and the negative value of ΔG^{o}_{ads} designate impulsive adsorption and strong interaction of polymer onto the surface. The calculated ΔG^{o}_{ads} are (− 38.81 KJ mol^{-1}), (− 37.25 KJ $mol^{-1)}$ and (− 36.13 KJ $mol^{-1)}$ from Freundlich, Langmuir and Timken, respectively, indicating that the adsorption of polyurethane on the superficial may be chemisorption (Fredric 2004). For more understanding of the adsorption of polymer on the iron surface, some kinetic models are considered for testing this behavior. Figure 13a displays the pseudo-first-order kinetic model, and it is clearly noticed that the correlation coefficient $R^2 = 0.5275$ which means that this model is not a good fit for the adsorption of polyurethane on iron artifacts. In the case of the pseudo-second-order kinetic model since $R^2 = 0.9986$, as publicized in Fig. 13b, that means this model is in a good fit with the gained results of polyurethane adsorption on the iron artifact surface. Figure 13c shows the Elovich model with obtained correlation coefficients of about $R^2 = 0.9570$, this value is in between the two values of both pseudo-first and second-order models. These results authorize that the mode of adsorption of polyurethane on the iron artifact is chemisorption and the whole adsorption process obeys the pseudo-second-order model (Xu et al. 2016).

Conclusion

The decorative ironworks in the tomb of Suleiman Pasha Al-Faransawi were made of wrought iron and cast iron. They were painted with red paints that were subjected to degradation as the iron underneath was corroded, thus required a new protective coat. Corrosion of the decorative ironworks happens where the iron is left uncoated for a long time. It is important that the coating is continuous, as holes and cracks allow the development of electrochemical cells in which an anodic area develops under the film around the hole, causing corrosion to be increased. It was concluded that:

- The obtained results of polarization and impedance data show that polyurethane inhibits the weathering of iron through the adsorbed film at the surface.
- The adsorption isotherm and adsorption kinetics concluded that the polymer adsorption is obeyed the Freundlich isotherm
- The kinetics of the process is agreed with the pseudo-second-order kinetics.
- These results authorize that the mode of adsorption of polyurethane on the iron artifact is chemisorption and the whole adsorption process obeys the pseudo-second-order model.
- OCP measurements assign the noblest Ecorr to the 2% polyurethane followed by 1% polyurethane and then the blank.
- Polyurethane is acting as a good protective coating for the decorative ironworks exposed in an uncontrolled environment.
- The 2% is considered as the recommended dose for this polymer for minimum corrosion rate of the ironworks.

Abbreviations

XRD: X-ray diffraction; EIS: Electrochemical impedance spectroscopy; OCP: Open circuit potential.

Acknowledgements

Not applicable.

Authors' contributions

YR, MA, and AE conceived and planned the presented research. AE (corresponding author) confirms that all listed authors have approved the manuscript before submission. MA performed the technical analysis. YR carried out the experiments. All authors read and approved the final manuscript.

Funding

Not applicable.

Availability of data and materials

The datasets used and/or analyzed during the current study are available from the corresponding author on reasonable request.

Declarations

Ethics approval and consent to participate

Not applicable.

Consent for publication

Not applicable.

Competing interests

The authors declare that they have no competing interests.

Author details

[1] Chemical Engineering Department, Canal High Institute of Engineering and Technology, Higher Institute of Engineering and Technology Tanta, Tanta, Egypt. [2] Conservation Department, Faculty of Archaeology, Damietta University, Damietta El-Gadeeda City 34511, Damietta Governorate, Egypt. [3] Electrochemistry and Corrosion Lab., Physical Chemistry Department, National Research Centre, El-Bohouth St. 33, Dokki, P.O. 12622, Giza, Egypt.

Received: 26 November 2020 Accepted: 24 March 2021
Published online: 01 April 2021

References

Abdel-Karim AM, El-Shamy AM, Megahed MM, Kalmouch A (2018) Evaluation the inhibition efficiency of a new inhibitor on leaded bronze statues from Yemen. Arct J 71(1):2–33

Akindoyo JO, Beg MDH, Ghazali S, Islam MR, Jeyaratnama N, Yuvaraj AR (2016) Polyurethane types, synthesis and applications a review. R Soc Chem 6:114453–114482
Barker D (2006) Metals. In: May E, Jones M (eds) Conservation science. Heritage Materials, The Royal Society of Chemistry, Cambridge
Behnam MM, Davamia P, Varahram N (2010) Effect of cooling rate on microstructure and mechanical properties of gray cast iron. Mater Sci Eng A 528(2):583–588
Blackney K (2002) Cleaning historic ironwork for repainting. The Building Conservation Directory, Cathedral Communications Limited, Tisbury. http://www.buildingconservation.com/articles/cleaningironwork/cleaningironwork.htm. Accessed 3 June 2019
Bramfitt BL, Benscoter AO (2002) Metallographer's guide: practices and procedures for irons and steels
Bussell M (2007) Use of iron and steel in buildings. In: Forsyth M (ed) Structures and construction in historic building conservation. Blackwell Publishing Ltd, pp 173–191
Campbell JWP, Tutton M (2013) Staircases: history, repair, and conservation. Routledge, London
Cardarelli F (2008) Materials handbook: a concise desktop reference, 2nd edn. Springer
Colson A, Stephenson A, Xu N, Li W, Krishnan B (2015) Polyurethane adhesives and sealants based on hydrophobic polyols. American Chemistry Council
Cronyn JM (1992) The elements of archaeological conservation. Routledge, London
Davey A (2013) Maintenance and repair techniques for traditional cast ironwork. Historic Scotland
Donnelly J (2009) Iron: the repair of wrought and cast ironwork. Department of the Arts, Heritage and the Gaeltacht
Elban WL, Borst MA, Roubachewsky NM, Kemp EL, Tice PC (1998) Metallurgical assessment of historic wrought iron: U.S. Custom House, Wheeling, West Virginia. Assoc Preserv Technol 29:27–34
El-Shamy AM, Zohdy KM, El-Dahan HA (2016) Control of corrosion and microbial corrosion of steel pipelines in salty environment by polyacrylamide. Ind Chem 2:2. https://doi.org/10.4172/2469-9764.1000120
El-Shamy AM, El-Hadek MA, Nassef AE, El-Bindary RA (2020) Optimization of the influencing variables on the corrosion property of steel alloy 4130 in 3.5 wt.% NaCl solution. J Chem 2020:9212491. https://doi.org/10.1155/2020/9212491 (**in press**)
Fredric T (2004) High-temperature corrosion of cast irons and steels. Chalmers University of Technology
Gayle M, Look DW, Waite JG (1992) Metals in America's historic buildings. Preservation Assistance Division, National Park Service, U.S. Department of the Interior, Washington, DC
Hawkes PW (1979) Paints for architectural cast iron. Bull Assoc Preserv Technol 11:17–36
Howell JS (1987) Architectural cast iron: design and restoration. J Assoc Preserv Technol 19:51–55
Logan J (1995) Care and cleaning of iron. Canadian Conservation Center, Ottawa, Canada: CCI Notes 9/6
Makar JM, Desnoyers R, Mcdonald SE (2001) Failure modes and mechanisms in gray cast iron pipes. In: Underground infrastructure research, Waterloo, Ontario
Matero FG (1994) Conservation of architectural metalwork: historical approaches to the surface treatment of iron. In: Scott DA, Podany J, Considine B (eds) Ancient and historic metals: conservation and scientific research. Getty Conservation Institute, Los Angeles, pp 197–228
Mitchell D (2009) Ornamental cast iron. The Building Conservation Directory. http://www.buildingconservation.com/articles/orncastiron/orncastiron.htm. Accessed 24 June 2019
Reda Y, El-Shamy AM, Eessaa AK (2018) Effect of hydrogen embrittlement on the microstructures of electroplated steel alloy 4130. Ain Shams Eng J 9(4):2973–2982. https://doi.org/10.1016/j.asej.2018.08.004
Reda Y, El-Shamy AM, Zohdy KM, Eessaa AK (2020) Instrument of chloride ions on the pitting corrosion of electroplated steel alloy 4130. Ain Shams Eng J 11:191–199. https://doi.org/10.1016/j.asej.2019.09.002
Scott DA (1991) Metallography and microstructure of ancient and historic metals. The Getty Conservation Institute; The J. Paul Getty Museum, Los Angeles
Scott DA, Eggert G (2009) Iron and steel in art: corrosion, colorants, conservation. Archetype Publications, London
Selwyn L (2004) Overview of archaeological iron: the corrosion problem, key factors affecting treatment, and gaps in current knowledge. In: Ashton J, Hallam D (eds) Metal 2004: Proceedings of interim meeting of the ICOM-CC Metal WG, National Museum of Australia, Canberra, pp 294–306
Shehata MF, El-Shamy AM, Zohdy KM, Sherif ESM, Zein El Abedin S (2020) Studies on the antibacterial influence of two ionic liquids and their corrosion inhibition performance. Appl Sci 10(4):1444–1453. https://doi.org/10.3390/app10041444
Taylor J (2000) Wrought Ironwork. The Building Conservation Directory. http://www.buildingconservation.com/articles/wroughtiron/wrought2000.htm. Accessed 24 June 2019
Thompson H, Folkard C (2001) DK eyewitness travel guide: Egypt. Dorling Kindersley limited, London
US National Park Service (1991) 27 Preservation Briefs. In: Waite JG (ed) Technical Preservation Services, The Maintenance and Repair of Architectural Cast Iron, National Park Service, US Department of the Interior. http://www.nps.gov/tps/how-to-preserve/briefs/27-cast-iron.htm. Accessed 21 June 2019
Xu Q, Gao K, Lv W, Pang X (2016) Effects of alloyed Cr and Cu on the corrosion behavior of low-alloy steel in a simulated groundwater solution. Corro Sci 102:11–124
Zohdy KM, El-Shamy AM, Kalmouch A, Gad EAM (2019) The corrosion inhibition of (2Z,2′ Z)-4,4′-(1,2-phenylene bis (azanediyl)) bis (4-oxobut-2-enoic acid) for carbon steel in acidic media using DFT. Egypt J Petrol 28(4):355–359. https://doi.org/10.1016/j.ejpe.2019.07.001

Publisher's Note